Eur. Phys. J. B **7**, 347–357 (1999)

THE EUROPEAN PHYSICAL JOURNAL B

EDP Sciences

Structural origin of magnetic anisotropy in Co-Pt alloy films probed by polarized XAFS

C. Meneghini[1,5], M. Maret[2,a], V. Parasote[2], M.C. Cadeville[2], J.L. Hazemann[3], R. Cortes[4], and S. Colonna[5]

[1] INFN, Laboratori Nazionali di Frascati, P.O. Box 13, 00044 Frascati Roma, Italy
[2] Institut de Physique et Chimie des Matériaux de Strasbourg, GEMM[b], 23 rue du Loess, 67037 Strasbourg Cedex, France
[3] Laboratoire de Cristallographie, CNRS, B.P. 166, 38042 Grenoble, France
[4] Laboratoire de Physique des Liquides et Électrochimie[c], Université Pierre et Marie Curie, 75230 Paris Cedex 05, France
[5] INFM – GILDA CRG c/o ESRF, B.P. 220, 38043 Grenoble, France

Received: 29 April 1998 / Revised: 27 July 1998 / Accepted: 31 August 1998

Abstract. Polarized X-ray absorption fine structure (XAFS) measurements at the Co K and Pt L_3 edges show that the perpendicular magnetic anisotropy found in epitaxial fcc $CoPt_3$ (111) films stems from the existence of anisotropic local ordering. Such ordering, induced during the codeposition process and dependent on the growth temperature, is characterized by preferential CoCo pairs in the film plane, balanced by preferential CoPt pairs out of the plane, resulting from some Co 2D-segregation. Polarized XAFS at the Pt edge reveals similar anisotropic local ordering in epitaxial hcp Co_3Pt (0001) films exhibiting a larger magnetocrystalline anisotropy compared to that of bulk hcp Co. Besides, a polarization dependence of the Co XANES profile is observed only for the Co_3Pt films exhibiting hcp symmetry.

PACS. 75.70.-i Magnetic films and multilayers – 78.70.Dm X-ray absorption and absorption edges – 75.30.Gw Anisotropy

1 Introduction

Over the last few years, the Co-Pt alloy films have been extensively studied. Owing to their strong perpendicular magnetic anisotropy (PMA) and their enhanced Kerr rotation at short wavelengths compared to the Co/Pt multilayers or the currently used TbFeCo films, they are potential materials for high density magneto-optic recording [1, 2]. Therefore, the understanding of PMA which stems from an intrinsic magnetocrystalline anisotropy overcoming the extrinsic shape anisotropy, is a prerequisite to use the Co-Pt alloy films in magneto-optic industry.

Near the $CoPt_3$ composition, the magnetic anisotropy of alloy films, prepared by molecular beam epitaxy [3,4] or sputtering [5], is strongly dependent on the growth temperature. The strongest PMA is found in MBE-films codeposited near 690 K; this temperature is lowered of 100 K in sputtered films. X-ray diffraction measurements have shown that the epitaxial $CoPt_3$ (111) films with strong PMA, grown on mica substrates with a Ru (0001) buffer or sapphire substrates, present a disordered fcc structure. In contrast, the disappearance of PMA in $CoPt_3$ (111) films grown at temperatures higher than 750 K is clearly related to the existence of a $L1_2$-type long range ordering. In fully $L1_2$-ordered films, all (111) planes have the same composition $CoPt_3$, and the nearest neighbor environments of Co and Pt atoms are isotropic (*i.e.* a Pt atom is surrounded by 2 Co atoms and 4 Pt atoms both in the same (111) plane and out of this plane, and a Co atom is surrounded in and out of the plane each by 6 Pt atoms).

The occurrence of strong PMA with 100% remanence in disordered fcc $CoPt_3$ films indicates that the magnetization along the [111] growth direction is easier than along the three other axes, namely $[\bar{1}11]$, $[\bar{1}\bar{1}1]$ and $[1\bar{1}1]$, which in a perfect disordered fcc lattice are equivalent to [111]. The discovery of chemical long-range ordering(LRO) along the c axis in hcp Co_3Pt (0001) films grown on sapphire [6] or mica substrates [7,8] which enhances PMA, suggests the existence of similar effects as a structural source of PMA in fcc $CoPt_3$ (111) films. But these effects would be restricted on a local range since no X-ray diffraction intensity was measured at the half of the $\mathbf{q}_{111}$ scattering vector. Such anisotropic ordering has been already proposed, steming either from heterogeneities creating boundaries between Co-rich and Pt-rich regions [2] or from a magnetically driven miscibility gap leading to Co clustering [3].

Here, the objective of the X-ray absorption fine structure (XAFS) measurements is to probe such anisotropic local order effects in fcc $CoPt_3$ (111) and also in hcp

[a] e-mail: Mireille.Maret@uni-konstanz.de
[b] UMR 46 CNRS-ULP
[c] UPR 15 CNRS

$\sim$ Co_3Pt (0001) films, and to relate them to the appearance of PMA. The polarization sensitivity of the XAFS signal [9] allows us really to sort out neighbor atoms that are located in the same (111) plane as the absorbing atom or out of this plane. Such technique was already used for investigating structural anisotropy in amorphous rare earth-transition metal alloys as a source of magnetic anisotropy [10], and recently in a thin polycristalline $Co_{28}Pt_{72}$ film grown at 573 K [11]. However, in the latter work, the analysis of the XAFS spectra is not fully convincing; on the one hand, the differences between the in-plane and out-of-plane CoPt (or PtCo) pair coordination numbers extracted at both Co-K and the Pt-L_3 edges are comparable, even though they should be in the ratio of the atomic concentrations, on the other hand the contribution of the isotropic term [9] at the Pt-L_3 edge is not considered.

In this paper, we present, first, the measurements performed at the Co-K and Pt-L_3 edges in two fcc $CoPt_3$ films exhibiting different magnetic behaviours. Due to the enhancement of atomic changes around the minority atoms and as already mentioned to the weakened polarization sensitivity of XAFS at the Pt-L_3 edge, chemical anisotropic ordering is clearly evidenced from the Co-K edge spectra measured under glancing and normal incidences (a part of these results was shortly presented in [12]). Then, we analyze the XAFS spectra performed in hcp $\sim$ Co_3Pt films, among which only one presents a chemical long-range order along the c axis. The higher magnetocrystalline anisotropy of no long-range ordered Co_3Pt films compared to that of bulk hcp Co is shown to be also related to anisotropic local ordering similar to that found in $CoPt_3$ films. Such order is characterized by homoatomic and heterotamic pairs preferentially oriented in the film plane and out of this plane, respectively. It differs from those established in the fcc $L1_2$ or hcp DO_{19}-type ordered A_3B bulk crystals, where A and B atoms have the same nearest neighbours in the (111) or (0001) planes than out of these planes. Such anisotropic ordering is really induced by the MBE technique and would be essentially driven by two effects during co-deposition: one relying on Pt segregation at the advancing surface and the other related to dominant surface diffusion compared to bulk diffusion in a growth temperature range around 690 K.

2 Sample preparation and characterization

Co_xPt_{1-x} films of 400–500 Å thickness were deposited at different temperatures, T_g, ranging from 500 to 750 K in a 10^{-10} torr vacuum onto a 150 Å Ru (0001) buffer grown at 900 K on mica (001) substrate. Electron gun sources were used for both Co and Pt with deposition rates in the range 0.05–0.2 Å/s monitored by two quartz balances. The alloy films were covered by a 20 Å protective Pt layer deposited at room temperature.

The structure of epitaxial films was previously investigated by X-ray diffraction measurements and their magnetic properties investigated using a SQUID magnetometer [4,7]. From the parallel and perpendicular magnetization hysteresis loops measured at 30 K, the effective and uniaxial anisotropy energies (K_{eff} and $K_u = K_{eff} + 0.5\mu_o M_s^2$) were determined. Here, we summarized the main features of the films studied by polarized XAFS.

In the Pt-rich epitaxial films grown at 690 and 800 K, the Pt atomic fractions are equal to 0.75 and 0.68 ($\pm$ 0.02) respectively, *i.e.* within the stability range of the $L1_2$ structure [13]. The stacking sequence is fcc with some stacking faults, but only the film grown at 800 K exhibits partial $L1_2$-type ordering, characterized by a chemical LRO parameter close to 0.2 [14]. The effective magnetic anisotropies (K_{eff}) and the shape anisotropies ($0.5\mu_o M_s^2$) are 0.8 and 0.2 MJ/m^3 for the film grown at 690 K and -0.03 and 0.2 MJ/m^3 for the film grown at 800 K. Therefore only the film grown at 690 K presents strong PMA. X-ray asymmetric reflection measurements have shown a deformation of the fcc stacking observed in the film grown at 690 K. Strain relaxation was mostly achieved after ex-situ annealing for one day at 690 K, related to an increase of the interatomic distance between (111) planes together with a complete disappearance of PMA.

In the Co-rich films grown between 650 and 750 K, the stacking sequence is predominantly hcp with a volume fraction close to 90%, while the minority fcc stacking includes many stacking faults. One film of composition $Co_{82}Pt_{18}$, grown at T_g = 690 K and exhibiting a mosaic spread of 1.1°, presents a chemical LRO only along the [0001] growth direction, steming from alternate Co-enriched and Pt-enriched planes. The chemical LRO parameter, associated to this uniaxial ordering, is defined as $(\tau_1 - \tau_2)/2x_{\mathrm{Pt}}$, where τ_1 and τ_2 are the occupancy rates of Pt atoms on the Pt-rich and Pt-poor alternate (0001) planes and x_{Pt} is the Pt alloy fraction. It was deduced from the ratio of the 0001 and 0002 reflection intensities and equal to 0.54, *i.e.* corresponding to Pt compositions of the two alternate planes equal to 28 and 8%. The structural quality of three other studied films of composition $Co_{75}Pt_{25}$ is significantly lower with a mosaic spread of 1.9°, resulting from the lower quality of a Ru buffer. We suggest that the presence of an increased number of steps related to a larger mosaic spread reduces the spatial coherence of the Co-rich and Co-poor planes stacking. This would explain the absence of the (0001) superstructure peak in the X-ray patterns of these $Co_{75}Pt_{25}$ films.

All the K_{eff} constants given in Table 3 are positive indicating an easy axis of magnetization along the [0001] growth direction. But the PMA is really enhanced by the chemical long range ordering along the c axis, characterized by heterotamic pairs preferentially out of the film plane, between Co atoms of large atomic moment and Pt atoms of strong spin-orbit coupling. The K_u values, deduced from the effective and shape anisotropies, are equal to 1.5 MJ/m^3 for the films grown at 650 and 700 K and then significantly larger than that for the film grown at 750 K, equal to 1.1 MJ/m^3 (*i.e.* close to that of the pure hcp Co equal to 1 MJ/m^3). This difference could be also

attributed to the existence of anisotropic local order in the films grown below 750 K.

3 Experimental technique and data analysis

Three series of polarized XAFS measurements were performed under glancing and normal incidences. The first series was carried out at the European Synchrotron Radiation facilities (ESRF, Grenoble) on the bending magnet CRG-IF, at both Pt L_3 ($E_o = 11563$ eV) and Co K ($E_o = 7720$ eV) edges, with a Si (311) double-crystal monochromator. XAFS spectra were collected using a total electron yield (TEY) detector with He gas flow working at liquid nitrogen temperature (described in [15]). In order to avoid Bragg peaks the samples were mounted on a special 360° rotating plate using an Ag lake to ensure the electrical contact. The sample holder is inclined of 8° with respect to the incoming beam direction. It can be oriented with the electric field vector **E** strictly in the film plane for the in-plane polarization measurements, or it can be rotated by 90° around the incoming beam direction to realize the out-of-plane polarization geometry with **E** at 8° from the surface normal.

The second series was performed at the "Laboratoire pour l'Utilisation du Rayonnement Électromagnétique" (LURE, Orsay) on the XAFS2 beamline at 10 K at the Co K edge and the third series at the ERSF beamline CRG-GILDA [16] at 70 K at the Pt L_3 edge. In these two series, the alloy films are vertical and the spectra are collected in fluorescence mode using 7-elements Ge detectors, for different angles γ between the surface normal and the incident photon beam; namely on XAFS2 γ is equal to 0 and 84° and on GILDA γ equal to 15 and 75°, corresponding to the in-plane and out-of-plane polarizations respectively.

XAFS spectra were analyzed using the software package for Exafs Data Extraction and Modeling written by Aberdam [17]. XAFS spectra are first renormalized according to the edge jump and the atomic absorption computed with the Cromer and Liberman fPrime program [18]. The fine structure signal $\chi(k)$ is given by $(\mu(k) - \mu_o(k))/\mu_o(k)$, where k is the photoelectron wave vector, $k = \sqrt{(2m/\hbar^2)(E - E_{o,j})}$, $E_{o,j}$ the energy origin varying from shell to shell and $\mu_o(k)$ the atomic absorption simulated by cubic splines above 2 Å^{-1}. Fourier transforms of the k-weighted function $\chi(k)$ were calculated using a Kaiser apodization function. The nearest neighbour XAFS oscillations are isolated by back Fourier transforming the first F.T. peak and the structural parameters are obtained by fitting such filtered signal to the standard XAFS formula [19]:

$$\chi(k) = \sum_j \frac{N_j^*}{kR_j^2} F_j(k) \exp(-2k^2\sigma_j^2) \times \exp\left(-\frac{2R_j}{\lambda(k)}\right) \sin(2kR_j + \phi_j(k)) \quad (1)$$

where R_j is the mean distance between the absorbing atom and the jth shell, $F_j(k)$ the backscattering amplitude of the jth neighbor atom, σ_j the rms deviation from the average distance R_j, $\lambda(k)$ the mean free path of photoelectron varying as $\lambda(k) = \Gamma/k$ and $\phi_j(k)$ the total phase shift. For nonisotropic systems N_j^* is the polarization dependent effective coordination number [20]:

$$N_j^* = 3\sum_{i=1}^{N_j} \cos^2 \alpha_{ji} \quad \text{for Co K edge,} \quad (2)$$

$$N_j^* = 0.7N_j + 0.9\sum_{i=1}^{N_j} \cos^2 \alpha_{ji} \quad \text{for Pt } L_3 \text{ edge.} \quad (3)$$

At the Pt L_3 edge, the polarization sensitivity of XAFS is thus weakened by the isotropic term $0.7N_j$ and α_{ji} is the angle between **E** and the bond between the absorbing atom and the ith neighbor atom of the jth shell.

For the study of the first neighbor shell in epitaxial (111) or (0001) films, under glancing incidence (*i.e.* **E** very close to the surface normal and large γ values) it can be assumed that only the first neighbors out of the (111) or (0001) plane containing the central atom, denoted $N_j^\perp$, contribute to the Co-edge filtered signal, thus:

$$N_j^* = N_j^\perp. \quad (4)$$

Under normal incidence (*i.e.* **E** in the film plane (CRG-IF) or γ equal to 0 in vertical geometry (XAFS2)), 75% in-plane ($N_j^\parallel$) and 25% out-of-plane first neighbors around the central atom participate in the Co-edge filtered signal, giving:

$$N_j^* = 0.75N_j^\parallel + 0.25N_j^\perp. \quad (5)$$

On GILDA, for $\gamma = 15°$

$$N_j^* = 0.695N_j^\parallel + 0.305N_j^\perp. \quad (6)$$

The transferability of the backscattering amplitudes and phase shift functions calculated by McKale *et al.* [21] were tested on the XAFS filtered signal of the first coordination shell for two reference compounds, a fcc disordered Co_3Pt bulk alloy ($a_{fcc} = 3.644$ Å) and a fcc partially $L1_2$-type ordered $CoPt_3$ alloy ($a_{fcc} = 3.854$ Å). The chemical LRO parameter in bulk $CoPt_3$ equal to 0.63 was deduced from the X-ray integrated intensities of the 100, 110, 200 and 220 reflections, corrected for Lorentz polarization and Debye-Waller factors. The average short-range order in the ordered $CoPt_3$ is deduced from this LRO parameter which is related to the occupancy rates of each species in the four sublattices describing the $L1_2$ structure (see Ref. [14]): *i.e.* a Co atom is surrounded by 1.8 Co and 10.2 Pt atoms, while a Pt atom is surrounded by 3.4 Co and 8.6 Pt atoms. In the disordered Co_3Pt, Co and Pt atoms have the same first neighbour environment, 9 Co and 3 Pt atoms. Furthermore, the analysis of the bulk filtered signals, expected as independent on the polarization geometry, allows the determination of $E_{o,j}$ for each shell j and the Γ parameters at both edges which are are kept fixed in fitting the filtered signals of the corresponding films to improve the reliability of the extracted structural parameters.

Table 1. Interatomic distances r_j, in-plane and out-of-plane coordination numbers, $N_j^{\parallel}$ and $N_j^{\perp}$, around an atom in (111) and (0001) film planes; the equivalence between the two perfect fcc and hcp stackings is straightforward from the normalized distances with respect to the first nearest neighbor distance, r_j/r_1.

fcc phase				hcp phase			
r_j	r_j/r_1	$N_j^{\parallel}$	$N_j^{\perp}$	r_j	r_j/r_1	$N_j^{\parallel}$	$N_j^{\perp}$
$a^{fcc}/\sqrt{2}$	1	6	6	a^{hcp}	1	6	6
a^{fcc}	$\sqrt{2}$	–	6	$\sqrt{2}a^{hcp}$	$\sqrt{2}$	–	6
–	–	–	–	c^{hcp}	$\sqrt{8/3}$	–	2
$\sqrt{3/2}a^{fcc}$	$\sqrt{3}$	6	18	$\sqrt{3}a^{hcp}$	$\sqrt{3}$	6	12
–	–	–	–	$\sqrt{11/3}a^{hcp}$	$\sqrt{11/3}$	–	12
$\sqrt{2}a^{fcc}$	2	6	6	$2a^{hcp}$	2	6	–

Based on the McKale'backscattering amplitudes and phase shift functions, it is worth describing the simulated Fourier transforms corresponding to a first shell of 12 Pt atoms (or 12 Co atoms) located at the same distance from a central Pt atom (chosen equal to 2.6 Å, with a Debye-Waller equal to 0.05 Å) and the same shells around a Co atom. As seen in Figure 1, the first peak of the Fourier transform corresponding to the CoPt (PtPt) pairs is splitted into two components separated by about 0.4 (0.5) Å; this splitting is artificial and typical of heavy backscatterer shells. In contrast, the FTs for the PtCo and CoCo first pairs present a simple peak. Consequently, a strong splitting of the first peak found in the FTs of the alloy films will be the signature of dominant Pt nearest neighbors.

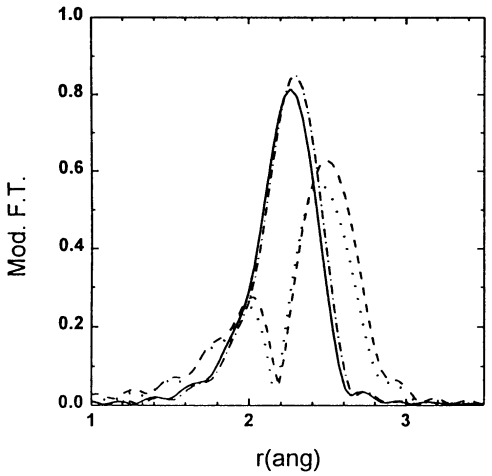

Fig. 1. Simulated Fourier transforms corresponding to first coordination shells of 12 Co atoms (solid curve) and 12 Pt atoms (dotted curve) around a Pt atom, and the same shells of 12 Co atoms (dot-dashed curve) and 12 Pt atoms (dashed curve) around Co atoms, calculated from the McKale backscattering amplitudes and shift functions.

4 Results and discussion

Figure 2 shows typical Co and Pt X-ray absorption near edge spectra (XANES), for in-plane and out-of-plane polarizations, measured for the hcp Co_3Pt and fcc $CoPt_3$ films, both grown at 690 K. A significant change in the Co K edge profile with photon beam polarization is observed for the LRO hcp Co_3Pt film. The same feature was also observed for a disordered hcp Co_3Pt grown at 700 K, but neither for the two studied fcc $CoPt_3$ films grown at 690 K and 800 K, nor for the fcc Co_3Pt reference compound. In contrast, the Pt XANES spectra of the fcc $CoPt_3$ and hcp Co_3Pt films are not very sensitive to polarization and it is certainly related to the isotropic term in the effective coordination number.

The strong polarization dependence of the XANES spectra observed only at the Co edge appears to be characteristic of the hcp symmetry rather than related to different in-plane and out-of-plane chemical environments. The comparison of the Co XANES spectra between the hcp and fcc films indicates that the strong differences are essentially between the two out-of-plane spectra. This result agrees with the fact that the atomic environments in the (0001) or (111) planes are identical, while they differ out of these planes, as indicated by the distances and numbers of in-plane and out-of-plane neighbors in the fcc (111) and hcp (0001) films listed in Table 1. However, the analysis and interpretation of the XANES spectra overcome the target of the present work, but these observations suggest some future research development.

4.1 $CoPt_3$ films

Figure 3 shows the Fourier transforms (F.T.) of the in-plane and out-of-plane spectra measured using TEY detection at the Pt L_3 edge for the polycrystalline $L1_2$-type ordered bulk alloy and the two MBE-grown (111) $CoPt_3$ films. The expected superimposition of both spectra observed for the isotropic bulk alloy probes that changes in the XAFS spectra with X-ray polarization measured for the MBE-grown films can be firmly attributed to different in-plane and out-of-plane atomic arrangements. For the two films (T_g = 690 and 800 K) the differences between the in-plane and out-of-plane F.T. are rather small. However, for the film grown at 690 K with strong PMA, they

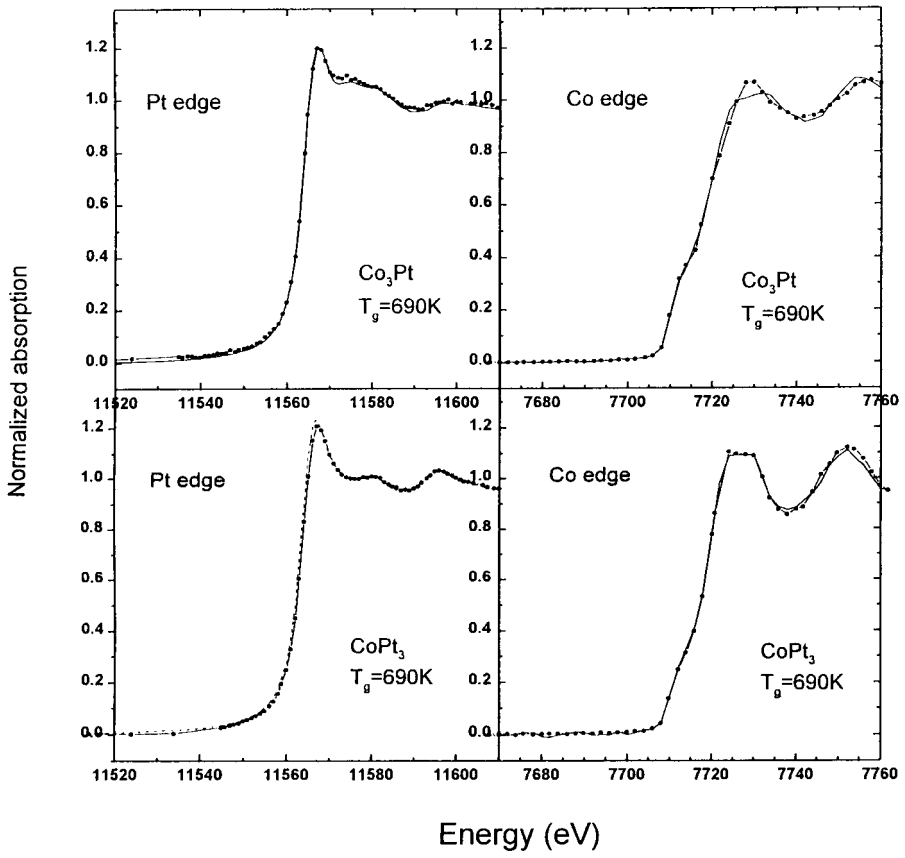

Fig. 2. Pt L_3 and Co K XANES spectra measured in a LRO hcp Co_3Pt (0001) film and a fcc $CoPt_3$ (111) film grown at 690 K, for out-of-plane (dotted curves) and in-plane (solid curves) polarizations.

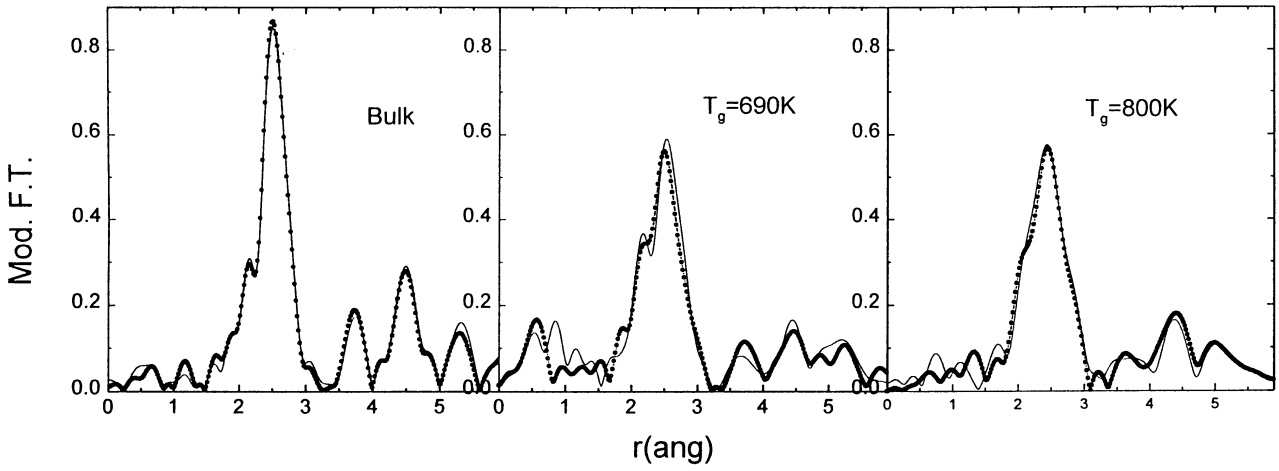

Fig. 3. Pt L_3 edge Fourier transforms of the $k\chi(k)$ spectra measured using TEY detection in a fcc $L1_2$-type ordered $CoPt_3$ bulk alloy and two epitaxial fcc $CoPt_3$ films grown at 690 and 800 K, for out-of-plane (dotted curves) and in-plane (solid curves) polarizations.

are slightly larger. The best fitting of the nearest neighbour filtered XAFS signals requires two sub-shells (PtCo and PtPt) whose parameters are summarized in Table 2. The error bars on the coordination numbers and disorder factors result mainly from strong correlation effects between these two parameters, shown by the normalized covariance matrix calculated by the modeling program; they are estimated from several satisfying fits by varying one of the parameter in a reasonable range. The differences between the out-of-plane and in-plane coordinations for each atomic pair, listed in Table 2 and characterizing the structural anisotropy, are obtained by taking account of the contributions of the out-of-plane atoms under normal incidence in equations (5, 6) and the isotropic term in equation (3), and normalizing the effective partial coordination numbers with respect to the real total numbers of in-plane and out-of-plane first neighbors equal to 6, as follows:

$$N_j^{\perp} - N_j^{\parallel} = 6\left[\left(\frac{N_j^*}{N^*}\right)_{E_\perp} - \left(\frac{N_j^*}{N^*}\right)_{E_\parallel}\right] / 0.9 \times 0.75 \quad (7)$$

on Pt edge

where the sums, $N^* = \sum_{j=\mathrm{Co,Pt}} N_j^*$, for out-of-plane ($E_\perp$) and in-plane ($E_\parallel$) polarization are equal. Consequently, the isotropic term is simply eliminated by making the differences between normalized effective coordination numbers. On GILDA beamline, the factor 0.75 is replaced by 0.67.

It turns out that the differences are really significant for the film grown at 690 K with strong PMA, such as the number of PtCo pairs is larger out-of-plane, while the number of PtPt pairs is larger in the film plane. For the film grown at 800 K, exhibiting $L1_2$-type ordering and magnetically isotropic, the weak differences between in-plane and out-of-plane coordinations are smaller than the uncertainties on the effective numbers, but the decrease of the disorder factors σ observed for the in-plane pairs is in agreement with the decrease of static disorder found in the $L1_2$-type ordered bulk alloys [23]. The extracted distances which exhibit no significant polarization dependence are in agreement with the average nearest neighbor distances deduced from our previous X-ray diffraction measurements equal to 2.724 and 2.71 Å for the films grown at 690 and 800 K, respectively.

As shown in the following, the analysis of the Co K spectra has allowed us to confirm the weak structural anisotropy extracted from the Pt edge data and to relate it with the occurrence of PMA. The Fourier transforms of the Co edge spectra are shown in Figure 4. For the film grown at 690 K, two series of XAFS spectra were collected using TEY and fluorescence detection on the CRG-IF and XAFS2 beamlines respectively. For the bulk alloy, the in-plane and out-of-plane Fourier transforms are similar emphasizing the accuracy of our measurements at the Co edge and the correctness of the data analysis. The intense F.T. peak observed at about at 5 Å stems from the contribution of the fourth neighbors located at a distance of $a_{fcc}\sqrt{2}$. This is a multiple scattering effect characteristic of fcc structures in which first and fourth shell are lined up with the absorber: the fourth shell XAFS signal is enhanced by the large forward scattering amplitude (focusing) at the intermediate first shell. In the bulk ordered alloy, this effect is well marked at the Co edge since Co atoms have 10.2 Pt first neighbors.

A strong polarization dependence of the Co F.T. spectra is now observed for the film grown at 690 K, clearly enhanced using TEY detection. The deviation between the two detection modes must be related to the different sampling depths. Using fluorescence mode, the whole thickness of the film (500 Å) is probed, while using TEY mode only the upper part of the film layer contributes to the XAFS signal, estimated from [22] at 200 Å. For the film grown at 690 K, strong changes are visible in both the first and the second neighbour regions and can be qualitatively explained. The marked splitting of the out-plane TF in the first neighbour region is the signature of dominant Pt first neighbours. Consequently, as shown by the increase of the peak at 5 Å when changing from in-plane to out-of-plane polarization, such Pt first neighbors enhance the focusing effect in the fourth neighbor shell. In contrast, the strong difference between the numbers of in-plane and out-of plane neighbors at a real distance of $\sqrt{3/2}a$ from the central atom (see Tab. 1), induces no significant change in the TF around 4.2 Å. A comparison of the Fourier transforms measured for the two films obtained by fluorescence shows an anisotropy in the first neighbour distribution clearly stronger in the film grown at 690 K.

The structural parameters corresponding to the best fits of the filtered signals by two subshells CoCo and CoPt are listed in Table 2, together with the differences between the out-of-plane and in-plane coordinations calculated using equation (7) but without the factor 0.9 related to the Pt edge. A structural anisotropy, characterized by a higher number of CoCo pairs in plane together with a higher number of CoPt pairs out-of-plane, is clearly observed for the film grown at 690 K, and still more marked using TEY detection (values in parentheses). This enhancement of the anisotropy between the two detection modes indicates that the upper layer of the alloy film (about 200 Å) probed by TEY is more anisotropic than the lower layer also detected by fluorescence.

This structural anisotropy gradient through the layer would be driven by the bulk diffusion that becomes the single diffusion process in the buried layers during the total codeposition time and tends to destroy the atomic arrangements built at the advancing surface. In fact the atomic arrangements at the advancing surface result mainly from Pt segregation, which as shown by the XAFS analysis yields the creation of Co enriched planar local regions alternated with Pt enriched local regions. Such stacking of compositionally different alternate planes along the growth direction [111] is absent in the $L1_2$-type equilibrium phase since all the (111) planes have the same composition. This point is also supported by the disappearance of chemical long range order along

Table 2. Structural parameters deduced from modeling Pt L_3 and Co K edge filtered XAFS signals, found in the two studied epitaxial fcc $CoPt_3$ films grown at 690 K and 800 K. At the Pt edge, data are obtained using TEY; at the Co edge, data are obtained using FY, and also using TEY for the film grown at 690 K (values in parentheses). The differences $N_j^{\perp} - N_j^{\parallel}$ are deduced from the effective coordination numbers using equation (7).

	out-of-plane polarization			in-plane polarization			
	r_j (Å)	N_j^*	σ_j(Å)$\times 10^{-2}$	r_j (Å)	N_j^*	σ_j(Å)$\times 10^{-2}$	$N_j^{\perp} - N_j^{\parallel}$
Pt-edge	$Co_{25}Pt_{75}$ grown at 690 K						
PtCo	2.68 ± 0.01	3.2 ± 0.3	6.3 ± 0.2	2.68 ± 0.01	2.8 ± 0.3	7.0 ± 0.3	0.4
PtPt	2.73 ± 0.01	8.1 ± 0.4	6.5 ± 0.2	2.74 ± 0.01	8.9 ± 0.4	6.5 ± 0.2	−0.4
Co-edge							
CoCo	2.69 ± 0.01	1.5 ± 0.5	3.0 ± 0.5	2.62 ± 0.01	2.5 ± 0.5	4.0 ± 2	−1.0
	(∼ 2.69)	(≤ 0.6)	(∼ 6.3)	(2.68 ± 0.01)	(3.7 ± 0.3)	(6.3 ± 0.3)	(−2)
CoPt	2.685 ± 0.005	9.3 ± 0.5	7.5 ± 0.5	2.715 ± 0.005	7.1 ± 0.5	7.0 ± 0.5	1.0
	(2.71 ± 0.01)	(10.5 ± 0.5)	(6.8 ± 0.2)	(2.71 ± 0.01)	(8.3 ± 0.5)	(6.9 ± 0.2)	(2)
Pt-edge	$Co_{32}Pt_{68}$ grown at 800 K						
PtCo	2.69 ± 0.01	3.8 ± 0.3	6.8 ± 0.2	2.68 ± 0.01	3.7 ± 0.3	6.6 ± 0.2	0.15
PtPt	2.73 ± 0.01	7.6 ± 0.4	6.1 ± 0.2	2.72 ± 0.01	8.0 ± 0.4	6.3 ± 0.3	−0.15
Co-edge							
CoCo	2.69 ± 0.005	2.2 ± 0.5	4.0 ± 0.5	2.71 ± 0.005	2.6 ± 0.5	4.0 ± 1.0	−0.3
CoPt	2.69 ± 0.005	9.1 ± 0.5	7.0 ± 0.5	2.675 ± 0.005	8.4 ± 0.5	7.0 ± 0.5	0.3

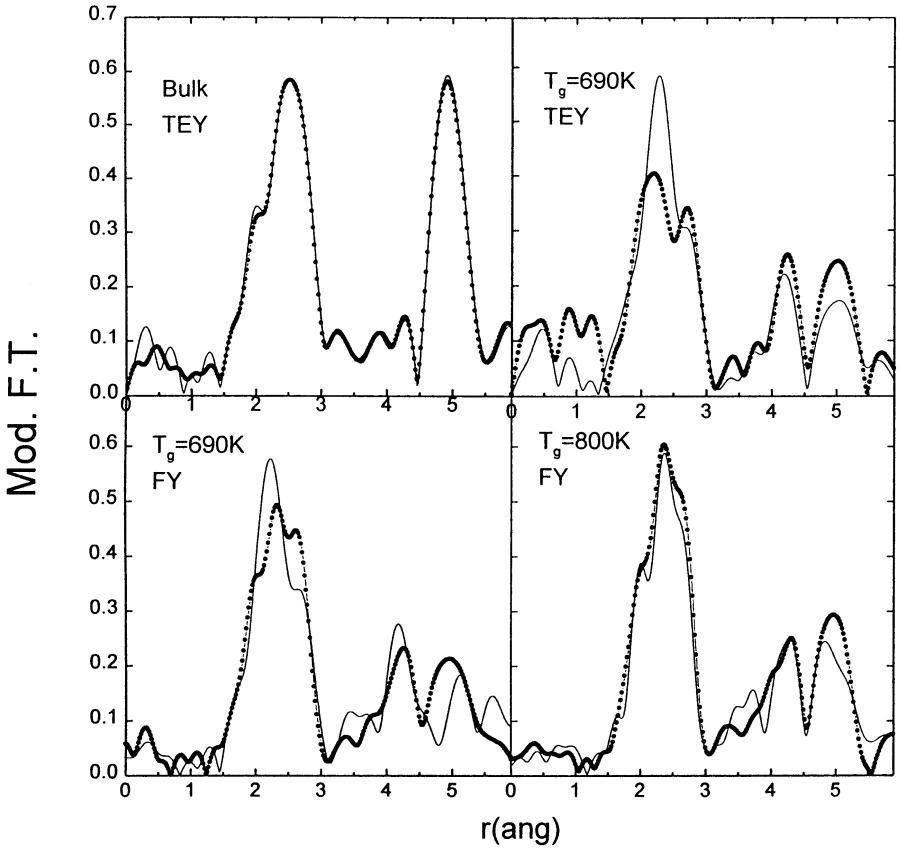

Fig. 4. Co K edge Fourier transforms of the $k\chi(k)$ spectra, measured using TEY detection in a fcc $L1_2$-type ordered $CoPt_3$ bulk alloy and the $CoPt_3$ film grown at 690 K , and using fluorescence yield (FY) detection in the two fcc $CoPt_3$ films grown at 690 and 800 K, for out-of-plane (dotted curves) and in-plane (solid curves) polarizations.

the c direction in (0001) hcp Co_3Pt films after *ex situ* annealing treatments performed at the same temperature as they were deposited. For the film grown at 800 K, a similar anisotropy but largely reduced is found at the Co-edge.

In contrast with the Pt-edge data, by changing the X-ray polarization, we observe significant variations of the CoCo and CoPt distances. For the film grown at 690 K, the CoCo distance extracted from fluorescence data is significantly smaller in the film plane in agreement with Co segregation, while the CoPt distance is somewhat larger in-plane. Such local shortening of the in-plane CoCo distances could explain the deformation of the fcc stacking measured by X-ray diffraction, revealed by an increase of the angle between the [111] and [113] directions with respect to that found in a ideal fcc phase [4]. For the ordered film grown at 800 K, the variations are smaller and of opposite sign compared with the other film; these results are consistent with the isotropic $L1_2$-type ordering and the quasi absence of Co segregation in plane.

Finally, in agreement with the Pt edge results, the analysis of the Co-edge data reveals that the strong PMA found in the film grown at 690 K is related to the existence of a well-defined anisotropic chemical local order, while in the film grown at 800 K magnetically isotropic, such structural anisotropy is markedly reduced.

4.2 $\sim$ Co_3Pt films

Using total yield detection, only the LRO hcp $Co_{82}Pt_{18}$ film grown at 690 K were measured at the Co-K and Pt-L_3 edges on the CRG-IF beamline (ESRF). Using fluorescence detection, Co XAFS spectra were recorded on the XAFS2 beamline (LURE) for a polycrystalline fcc Co_3Pt bulk alloy, and Pt spectra on the GILDA beamline (ESRF) for three predominantly hcp Co_3Pt films grown at 650, 700 and 750 K, one mostly fcc Co_3Pt film grown at 500 K and the polycrystalline fcc Co_3Pt bulk alloy. The k-weighted F.T. of the in-plane and out-of-plane Co spectra are shown in Figure 5. For the bulk alloy, the two spectra obtained using fluorescence detection are not identical, contrary to its isotropic structure; under glancing incidence the XAFS oscillations and consequently the peaks in the F.T. are clearly attenuated compared to the normal incidence. This deviation is related to self absorption effects under glancing incidence, occurring in the bulk alloy whose thickness is much larger than the penetration depth of the incoming photons. In contrast, such effects are not expected in thin films, 500 Å thick.

For the LRO film grown at 690 K measured using TEY detection, the differences observed in the first neighbor shell are small, however a slight narrowing of the first peak can be noted when changing from out-of-plane to in-plane polarization. In contrast, in the second neighbor shell, the peak at 4.1 Å is more pronounced under normal incidence. As seen in Table 1, this latter feature is specific to the hcp stacking sequence and results from the presence of in-plane next neighbors at a distance of $2a_{hcp}$ from the central atom and whose XAFS signal is amplified by the focusing effect at the intermediate first neighbors located at a_{hcp}; such collinear configurations are absent out of the film plane. The structural parameters extracted by modeling the filtered signal on the first coordination shell by two sub-shells CoCo and CoPt, using equation (1), are summarized in Table 3 for the two polarizations, together with the differences between the in-plane and out-of-plane coordination calculated as for the Pt rich films. In agreement with the existence of LRO determined by X-ray diffraction, a larger number of CoCo first neighbor pairs together with a smaller number of CoPt pairs are observed in the film plane. The difference, $N_j^{\perp} - N_j^{\parallel}$, estimated at 0.25 is between the value deduced from the chemical LRO parameter (0.15) and that calculated for a fully ordered film consisting of alternate Co pure and $Co_{64}Pt_{36}$ planes (0.47). The narrower first peak observed in the in-plane F.T. compared with the out-of plane F.T. is thus related to a smaller number of in-plane CoPt first pairs which produces a splitting of the first peak, as mentioned in Section 3.

The k-weighted F.T. of the Pt-L_3 spectra measured for the LRO film grown at 690 K (using TEY detection) and those obtained for three Co_3Pt films exhibiting no LRO from X-ray diffraction and grown at 650, 700 and 750 K (using fluorescence detection) are shown in Figure 6. For comparison, we present the curves for a mostly fcc (111) Co_3Pt film grown at 500 K and a polycrystalline fcc Co_3Pt bulk alloy, obtained only under normal incidence by fluorescence mode. The strong enhancement of the F.T. peak at 4 Å when changing from out-of-plane to in-plane polarization observed previously for the LRO film at the Co edge and characteristic of its hcp stacking, is only observable for this film (slightly shifted at 4.15 Å) and can be related to a larger number of in-plane PtPt pairs resulting from the chemical LRO along the c axis. As expected from the environments in the (0001) or (111) planes, the in-plane F.T. for the fcc or hcp alloy films are rather similar. The differences between the first neighbor shells of the in-plane and out-of-plane F.T. are small. For the LRO film a broadening of the first peak on its right side is visible when changing from out-of-plane to in-plane polarization, and can be attributed to a larger number of in-plane PtPt pairs, as confirmed by modeling the nearest neighbour filtered XAFS signal by two subshells PtCo and PtPt. The structural parameters extracted from the best fits are summarized in Table 3 together with the differences between the out-of-plane and in-plane atomic pair numbers. Except for the film deposited at the lowest temperature (650 K), we observe larger PtPt distances in the film plane than out of the plane; this trend, also true for the CoCo distances measured in the LRO film, is less marked for the PtCo pairs. Besides, these distances are in a good agreement with those deduced from the X-Ray diffraction measurements. The lattice parameters of the LRO $Co_{82}Pt_{18}$ film, $a = 2.6$ Å and $c = 4.18$ Å, lead to in-plane and out-of-plane first distances equal to 2.6 and 2.573 Å respectively, and for the $Co_{75}Pt_{25}$ film grown at 700 K, slightly richer in Pt, $a = 2.615$ Å and $c = 4.205$ Å correspond to in-plane and out-plane first distances equal to 2.615 Å and

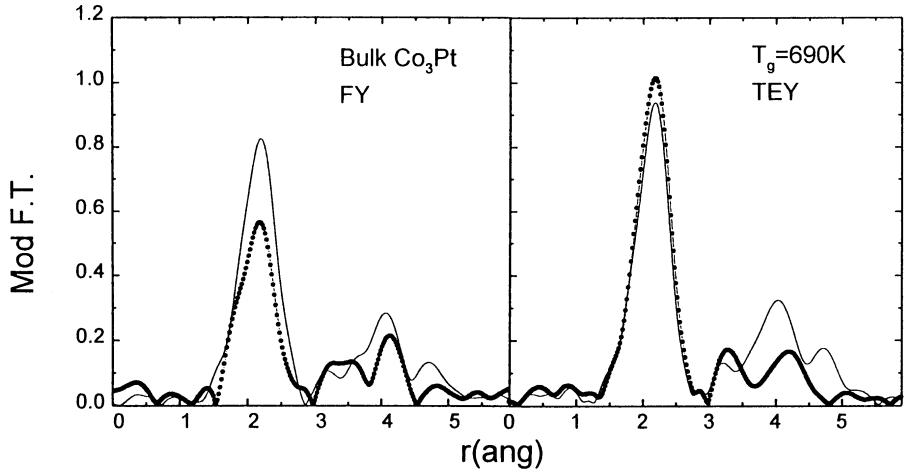

Fig. 5. Co K edge Fourier transforms of the $k\chi(k)$ spectra, measured using FY in a fcc Co_3Pt bulk alloy and using TEY in a long-range ordered hcp $Co_{82}Pt_{18}$ film grown at 690 K, for out-of-plane (dotted curves) and in-plane (solid curves) polarizations.

Table 3. Structural parameters deduced from modeling the XAFS filtered signals for a LRO hcp $Co_{82}Pt_{18}$ film grown at 690 K (at both Co and Pt edges) and three hcp $Co_{75}Pt_{25}$ films grown at 650, 700 and 750 K (at the Pt edge); the differences $N_j^{\perp} - N_j^{\parallel}$ are reported together with the effective and shape anisotropies, K_{eff} and $0.5\mu_o M_s^2$.

	out-of-plane polarization			in-plane polarization				
	r_j (Å)	N_j^*	σ_j(Å) $\times 10^{-2}$	r_j (Å)	N_j^*	σ_j(Å) $\times 10^{-2}$	$N_j^{\perp} - N_j^{\parallel}$	$K_{eff}/0.5\mu_o M_s^2$ (MJ/m^3)
Co-edge	$Co_{82}Pt_{18}$ grown at 690 K							
CoCo	2.55 ± 0.005	8.0 ± 0.2	8.0 ± 0.3	2.57 ± 0.005	8.4 ± 0.2	8.3 ± 0.3	-0.25	1.6/1
CoPt	2.56 ± 0.005	4.1 ± 0.3	7.5 ± 0.5	2.55 ± 0.01	3.7 ± 0.3	7.6 ± 0.5	$+0.25$	
Pt-edge								
PtCo	2.585 ± 0.005	8.0 ± 0.2	6.7 ± 0.3	2.59 ± 0.005	8.7 ± 0.4	7.6 ± 0.3	$+0.45$	
PtPt	2.57 ± 0.01	3.0 ± 0.5	$12. \pm 0.5$	2.59 ± 0.01	4.2 ± 0.5	11.8 ± 0.5	-0.45	
Pt-edge	$Co_{75}Pt_{25}$ grown at 650 K							
PtCo	2.61 ± 0.005	8.7 ± 0.3	7.9 ± 0.4	2.61 ± 0.005	8.5 ± 0.3	7.7 ± 0.3	$+0.15$	0.85/0.7
PtPt	2.58 ± 0.01	5.5 ± 0.4	10.0 ± 0.5	2.58 ± 0.005	5.7 ± 0.4	10.0 ± 0.5	-0.15	
Pt-edge	$Co_{75}Pt_{25}$ grown at 700 K							
PtCo	2.605 ± 0.005	9.0 ± 0.2	7.3 ± 0.3	2.61 ± 0.005	8.8 ± 0.2	7.8 ± 0.3	$+0.25$	0.8/0.75
PtPt	2.575 ± 0.01	4.6 ± 0.4	9.0 ± 0.3	2.595 ± 0.01	5.0 ± 0.5	8.8 ± 0.3	-0.25	
Pt-edge	$Co_{75}Pt_{25}$ grown at 750 K							
PtCo	2.605 ± 0.005	8.0 ± 0.2	7.0 ± 0.3	2.61 ± 0.005	9.0 ± 0.2	8.0 ± 0.3	-0.1	0.5/0.6
PtPt	2.58 ± 0.01	5.1 ± 0.4	10.0 ± 0.5	2.595 ± 0.01	5.5 ± 0.5	11.0 ± 0.5	$+0.1$	

2.588 Å. For the films grown at 650 and 750 K only the c parameters were determined, equal to 4.209 and 4.125 Å.

The K_{eff} and $N_j^{\perp} - N_j^{\parallel}$ values in Table 3 probe that the enhancement of perpendicular anisotropy in the hcp films is correlated with an increase of structural anisotropy characterized by CoCo and PtPt pairs, preferentially in the film plane as already observed for the fcc Pt rich films. For the films grown at 650 and 700 K and exhibiting an uniaxial magnetocrystalline anisotropy ($K_u = K_{eff} + 0.5\mu_o M_s^2$) larger than the Co pure hcp phase (as given in Sect. 2), the differences $N_j^{\perp} - N_j^{\parallel}$ related to the PtCo pairs are positive, while for the film grown at 750 K, magnetically closer to the Co hcp phase, a small negative value is measured. In spite of the significant errors in the extracted coordination numbers mostly related to the strong correlation with the disorder factors σ_j, the use of the same detection mode and the same procedure for extracting the structural parameters give some reliability in the correlation established between the local structural anisotropy and the enhanced magnetocrystalline anisotropy found in the hcp Co_3Pt films.

A comparison with the Co data obtained for the LRO film indicates that as expected the structural anisotropy is clearly more marked at the edge of the minority atoms.

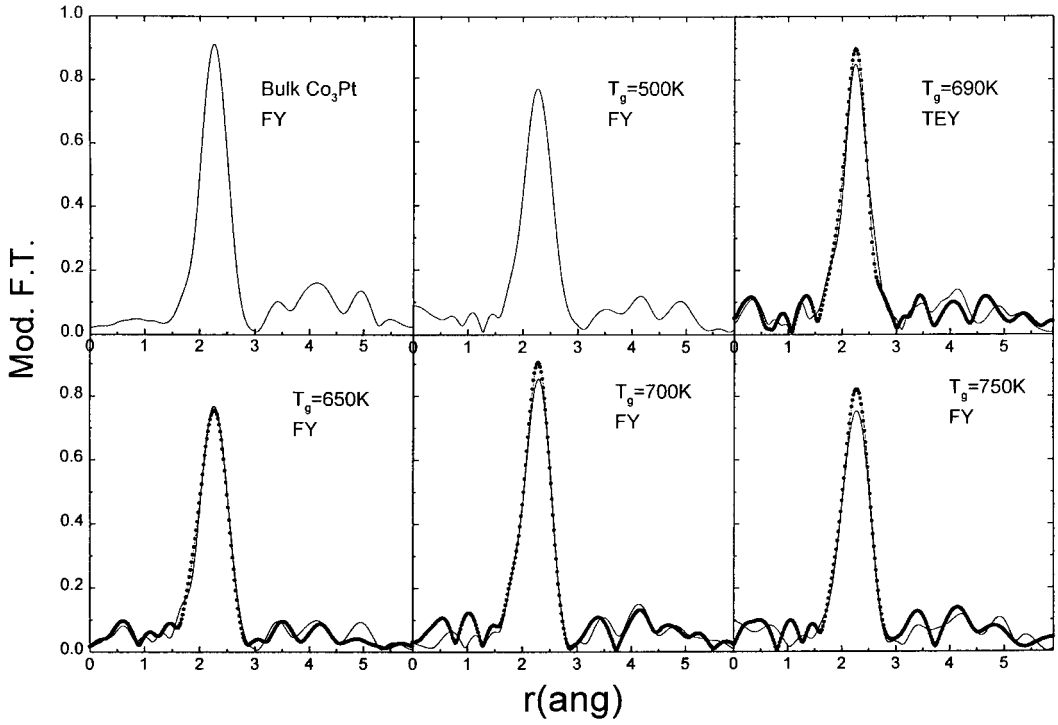

Fig. 6. Pt L_3 edge Fourier transforms of the $k\chi(k)$ spectra, measured using FY in a fcc Co_3Pt bulk alloy, a fcc Co_3Pt film grown at 500 K and three hcp Co_3Pt films grown at 650, 700 and 750 K and using TEY in a long-range ordered hcp $Co_{82}Pt_{18}$ film grown at 690 K, for out-of-plane (dotted curves) and in-plane (solid curves) polarizations.

However, the ratio between the differences measured at the two edges close to 2 is lower than that expected from the ratio of the atomic concentrations equal to 4.5. This deviation could be related again to the uncertainties in the extracted coordination numbers, but could really stem from an anisotropic local order around Co atoms enhanced with respect to that deduced from the LRO parameter and a weakened anisotropic order around Pt atoms.

5 Conclusions

The polarized XAFS measurements performed in two epitaxial fcc $CoPt_3$ (111) films, one grown at 690 K with strong perpendicular magnetic anisotropy and another grown at 800 K exhibiting a $L1_2$-type order and magnetically isotropic, reveal the existence of a local structural anisotropy strongly marked in the film grown at 690 K, characterized by preferential CoCo pairs in the film plane balanced with preferential heteroatomic pairs out of the plane. As expected, such effects are more pronounced at the edge of the minority atoms. In the film grown at 800 K, such structural anisotropy is attenuated and agrees with the appearance of the $L1_2$-type order, which is isotropic in the first coordination shell. Therefore, subtle changes at a local range can affect greatly the magnetic properties of these films.

The polarized XAFS measurements performed in an epitaxial hcp $Co_{82}Pt_{18}$ (0001) film, grown at 690 K and developing strong PMA, provide a description of the local anisotropic orders around the two species, associated with the chemical long-range ordering (LRO) along the growth direction measured by X-ray diffraction.

A last series of polarized XAFS measurements, performed in epitaxial hcp $Co_{75}Pt_{25}$ (0001) films grown at 650, 700 and 750 K and exhibiting no LRO, has allowed to correlate the growth temperature dependence of their magnetocrystalline anisotropy with the importance of anisotropic local order effects, similar to that found in the Pt-rich films.

References

1. D. Weller, H. Brändle, G.L. Gorman, C.J. Lin, H. Notarys, Appl. Phys. Lett. **61**, 2726 (1992).
2. D. Weller, H. Brändle, C. Chappert, J. Magn. Magn. Mat. **121**, 461 (1993).
3. P.W. Rooney, A.L. Shapiro, M.Q. Tran, F. Hellman, Phys. Rev. Lett. **75**, 1843 (1995).
4. M. Maret, M.C. Cadeville, R. Poinsot, A. Herr, E. Beaurepaire, C. Monier, J. Magn. Magn. Mat. **166**, 45 (1997).
5. M. Li, Z.H. Jiang, Z.Q. Zou, D.F. Shen, J. Magn. Magn. Mat. **176**, 331 (1997).
6. G.R. Harp, D. Weller, T.A. Rabedeau, R.F.C. Farrow, M.F. Toney, Phys. Rev. Lett. **71**, 2493 (1993).
7. M. Maret, M.C. Cadeville, W. Staiger, E. Beaurepaire, R. Poinsot, A. Herr, Thin Solid Films **275**, 224 (1996).
8. M. Maret, M.C. Cadeville, A. Herr, R. Poinsot, E. Beaurepaire, S. Lefebvre, M. Bessière, J. Magn. Magn. Mat. (to be published).

9. J. Stöhr in *X-Ray Absorption*, edited by Koninsberger, R. Prins (Wiley, New York, 1988) Vol. 92.
10. V.G. Harris, W.T. Elam, N.C. Koon in *High Density Digital Recording* edited by K.H.J. Buschow *et al.* (Kuwer Academic Publishers, Netherlands,1993).
11. T.A. Tyson, S.D. Conradon, R.F.C. Farrow, B.A. Jones, Phys. Rev. B **54**, R3702 (1996).
12. C. Meneghini, M. Maret, M.C. Cadeville, J.L. Hazemann, J. Phys. IV France **7**, C2-1115 (1997).
13. C. Leroux, M.C. Cadeville, V. Pierron-Bohnes, G, Inden, F, Hinz, J. Phys. F: Met. Phys. **18**, 2033 (1988).
14. M.C. Cadeville, V. Pierron-Bohnes, J.M. Sanchez, J. Phys.-Cond. **4**, 9053 (1992). The $L1_2$ (A_3B) structure can be represented by four interpenetrating cubic sublattices: three are equivalent and constructed from the centers of two opposite faces in the fcc lattice (sublattice 1, 2, 3) and the fourth consists of the corners of the fcc lattice (sublattice 4). The chemical LRO parameter is defined as $(P_{\rm Pt}^{1,2,3} - x_{\rm Pt})/(1 - \nu^{1,2,3})$ where $P_{\rm Pt}^{1,2,3}$ is the occupancy rate of the (1, 2, 3) sublattices by Pt atom, $x_{\rm Pt}$ the Pt alloy composition, and $\nu^{1,2,3}$ the ratio of the number of sites belonging to the sublattices 1, 2, 3 to the total number of sites in the fcc lattice (*i.e.* equal to 3/4), such as $x_{\rm Pt} = P_{\rm Pt}^{1,2,3}\nu^{1,2,3} + P_{\rm Pt}^{4}\nu^{4}$.
15. C. Revenant-Brizard, J.R. Regnard, J. Mimault, D. Duclos, J. Phys. IV France **7**, C2-325 (1997).
16. S. Pascarelli, F. Boscherini, F. D'Acapito, J. Hrdy, C. Meneghini, S. Mobilio, J. Synchrotron Rad. **3**, 147 (1996).
17. D. Aberdam, *Software package for Exafs data and Modeling* (Lab. Cristallographie, Grenoble, France, 1998).
18. D.T. Cromer, D. Liberman, J. Chem. Phys. **53**, 1891 (1970).
19. P.A. Lee, P.H. Citrin, P. Eisenberger, B.M. Kinkaid, Rev. Mod. Phys. **53**, 769 (1981).
20. Y. Iwasawa, J. Phys. IV France **7**, C2-67 (1997).
21. A.G. McKale, B.W. Veal, A.P. Paulikas, S.K. Chan, G.S. Knapp, J. Am. Chem. Soc. **110**, 3763 (1988).
22. T. Girardeau, J. Mimault, M. Jaouen, P. Chartier, G. Tourillon, Phys. Rev. B **46**, 7144 (1992).
23. H. Berg, J.B. Cohen, Met. Trans. **3**, 1797 (1972).